

Gamma-ray burst afterglow scaling relations for the full blast wave evolution

Hendrik J. van Eerten, Andrew I. MacFadyen

*Center for Cosmology and Particle Physics, Physics Department, New York University,
New York, NY 10003*

ABSTRACT

We demonstrate that gamma-ray burst afterglow spectra and light curves can be calculated for arbitrary explosion and radiation parameters by scaling the peak flux and the critical frequencies connecting different spectral regimes. Only one baseline calculation needs to be done for each jet opening angle and observer angle. These calculations are done numerically using high-resolution relativistic hydrodynamical afterglow blast wave simulations which include the two-dimensional dynamical features of expanding and decelerating afterglow blast waves. Any light curve can then be generated by applying scaling relations to the baseline calculations. As a result, it is now possible to fully fit for the shape of the jet break, e.g. at early time X-ray and optical frequencies. In addition, late-time radio calorimetry can be improved since the general shape of the transition into the Sedov-Taylor regime is now known for arbitrary explosion parameters so the exact moment when the Sedov-Taylor asymptote is reached in the light curve is no longer relevant. When calculating the baselines, we find that the synchrotron critical frequency ν_m and the cooling break frequency ν_c are strongly affected by the jet break. The ν_m temporal slope quickly drops to the steep late time Sedov-Taylor slope, while the cooling break ν_c first steepens then rises to meet the level of its shallow late time asymptote.

1. Introduction

Gamma-ray bursts (GRBs) are currently thought to result from the collapse of a massive star (Woosley 1993; MacFadyen & Woosley 1999) or a black hole-neutron star or neutron star-neutron star merger (e.g Eichler et al. 1989; Paczynski 1991). During these processes, a collimated relativistic blast wave is launched into the circumburst medium. The emission from the blast wave is commonly referred to as the *afterglow* of the burst and can be observed throughout the broadband spectrum as the blast wave decelerates and radiates at

progressively longer wavelengths (Meszaros & Rees 1997). Ever since the discovery of the first afterglows, these have been modeled successfully by combining a model for the blast wave dynamics with a synchrotron radiation model, where shock-accelerated particles radiate by interacting with a shock-generated magnetic field (e.g. Wijers et al. 1997; Wijers & Galama 1999; Frail et al. 2000; Panaitescu & Kumar 2002). Analytically tractable solutions for the dynamics are the self-similar Blandford-McKee (BM, Blandford & McKee 1976) and Sedov-von Neumann-Taylor (ST, Sedov 1959; Taylor 1950; Von Neumann 1961) solutions describing, respectively, the ultra-relativistic and non-relativistic phase of the blast wave evolution. At early time lateral spreading of the collimated jet has not yet set in and the outflow is purely radial, while at late times the jet will have become truly spherical, allowing the application of spherically symmetric solutions in both cases. As of yet, no analytical solution exists that fully captures the intermediate stage of the blast wave evolution, where the blast wave becomes transrelativistic, inhomogeneous along the shock front (Zhang & MacFadyen 2009; Van Eerten & MacFadyen 2011) and decollimates. Early attempts assumed a homogeneous shock front (Rhoads 1999) or spherical outflow (Huang et al. 1999), while even recently studies (e.g. Granot & Piran 2011) do not account for the radial structure of the jet.

The practical implications of the fact that the blast wave evolution is determined by a very small number of variables such that scalings between different explosion energies and circumburst density are possible were not fully realized until very recently. The scalings apply in the asymptotic self-similar limits, but also in the intermediate regime where the two-dimensional nature of jet decollimation is in full effect. This made it possible to use only a small set of simulations for different initial jet opening angles as a basis for a simulation-based fit code that can be applied to broadband afterglow data (Van Eerten et al. 2011).

But even though a complete recalculation of the dynamics of the blast wave is no longer necessary, there remained the equations of radiative transfer of (a representative number of) rays through the evolving jet, that have to be solved for each datapoint fit iteration. For a large number of iterations and datapoints this procedure remains computationally expensive and requires the use of a parallel computer.

The current study shows that the calculation time for a given light curve or spectrum can be further reduced. We demonstrate that scalability between blast waves has straightforward implications for scalability between light curves. In §2 we describe how the scaling relations for the dynamics of blast waves can be used to scale between light curves as well. We show that the scalings remain unchanged between the BM and ST regimes, and in §3 we demonstrate numerically that the scalings also hold in the intermediate regime and for off-axis observers. We discuss our findings in §4.

2. Full evolution scaling relations

We take the BM solution for the impulsive injection of an energy E_{iso} in a homogeneous medium with density $\rho_0 = n_0 m_p$ (with n_0 the number density and m_p the proton mass) as the initial condition. In this paper we will discuss only adiabatic blast waves exploding in a homogeneous interstellar medium, but all conclusions drawn here can be generalized to a stellar wind environment as well, which will be presented in a forthcoming publication. Only a small number of independent dimensionless combinations of the variables determining the fluid state at distance r , angle θ and source frame time t_e exists: $A \equiv r/ct_e$ (with c the speed of light), $B \equiv E_{iso} t_e^2 / \rho_0 r^5$, θ and θ_0 (the initial jet half-opening angle). Any fluid quantity can be expressed as a dimensionless combination (e.g. n/n_0 for the local number density n) and therefore as a function of the dimensionless variables. It follows that dimensionless fluid quantities are invariant under scalings that leave the dimensionless variables invariant. Van Eerten et al. (2011) made practical use of the scalings

$$\begin{aligned} E'_{iso} &= \kappa E_{iso}, \\ \rho'_0 &= \lambda \rho_0, \\ r' &= (\kappa/\lambda)^{1/3} r, \\ t'_e &= (\kappa/\lambda)^{1/3} t_e. \end{aligned} \tag{1}$$

The synchrotron emission spectra from the expanding blast wave can be described locally by a series of connecting power laws, see Fig. 1. Below the critical frequency ν_a the medium is optically thick due to synchrotron self-absorption. Critical frequency ν_m marks the synchrotron break frequency. Above the cooling-break frequency ν_c the accelerated electrons lose their energy too quickly to radiate fully at these frequencies. In detailed numerical models the evolution of the electron distribution is traced explicitly as it advects into the non-radiating, slow-moving and dilute downstream region, see e.g. Downes et al. (2002); Van Eerten et al. (2010). Alternatively, a steady state for the radiating fluid is assumed and the global cooling time t_c is equated to the duration of the explosion t_e (Sari et al. 1998). Both approaches lead to qualitatively the same behavior (Van Eerten et al. 2010).

Synchrotron radiation from shock-accelerated electrons in a shock-generated magnetic field is parametrized as follows: p denotes the power law slope of the shock-accelerated electron distribution, ϵ_B the fraction of magnetic energy relative to thermal energy, ϵ_e the fraction of downstream thermal energy density in the accelerated electrons, and ξ_N the fraction of the downstream particle number density that participates in the shock-acceleration process. Typical values for these parameters are $p \sim 2.5$, $\epsilon_B \sim 0.01$, $\epsilon_e \sim 0.1$, $\xi_N \sim 1$. These

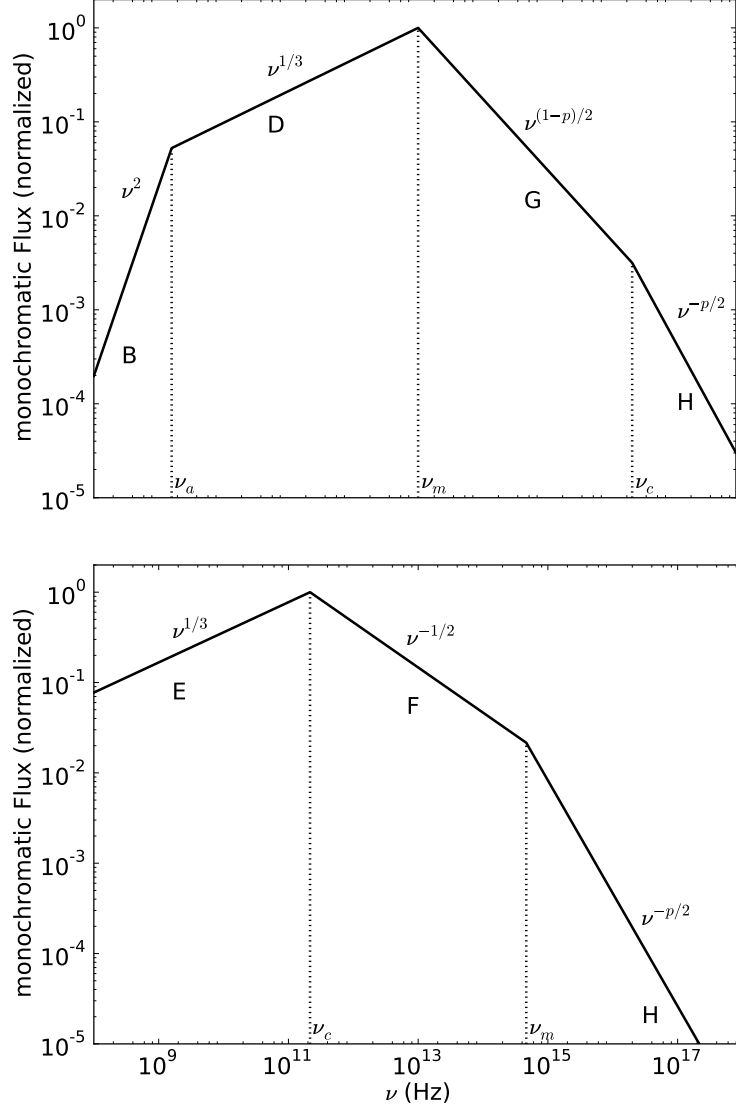


Fig. 1.— Synchrotron spectra with different orderings of the critical frequencies. The different power law segments are labeled by letters (following Granot & Sari 2002) and the spectral slopes are indicated in the plots.

parameters can be constrained from broadband afterglow data. At late times, maintaining $\xi_N \sim 1$ sometimes leads to unphysically low values for the lower cut-off Lorentz factor of the accelerated particle distribution (which determines ν_m). For a discussion, see e.g. Van Eerten et al. (2010), which explores (scale-invariant) evolution of ξ_N .

The synchrotron emission coefficient j_ν for a local distribution of particles follows $j_\nu \propto \xi_N n B f(\nu, \nu_m, \nu_c) / \gamma^2 (1 - \beta\mu)^2$ in the source frame, where number density n and magnetic field B are in the frame comoving with the fluid, γ denotes the fluid Lorentz factor, β the fluid velocity divided by c and μ the cosine of the angle between the fluid velocity and the observer direction. The function $f(\nu, \nu_m, \nu_c)$ is given by the synchrotron spectrum as shown in Fig 1 (without self-absorption, which is included in the absorption coefficient when enabled) and is normalized to one where the spectrum peaks. In the optically thin case, the observed flux is given by

$$F = \frac{1+z}{d_L^2} \int dV j_\nu / \gamma (1 - \beta\mu). \quad (2)$$

Here d_L is the luminosity distance and z the redshift. Although self-absorption is shown in Fig 1 for the case where $\nu_a < \nu_m < \nu_c$, we will concentrate on the case where observer frequency $\nu > \nu_a$ and leave a detailed treatment of self-absorption to future work. The leading order dependencies of the observed flux on the model parameters can be calculated from eq. 2, the shape of the synchrotron spectrum and a model for the dynamics that sets the radius of the afterglow blast wave as well as the post-shock values of n and B , ν_m and ν_c (the latter two via their dependence on the local fluid state, e.g. Sari et al. 1998). These are shown in table 1.

So far, no new arguments have been presented. *However, eq. 2 directly implies that scale invariance on the dynamical level leads to scale invariance for the flux within a given spectral regime* (e.g. when j_ν depends on ν_m , ν_c and ν according to a single combination of power laws). The table shows this explicitly for the various spectral regimes and the BM and ST limits. Additionally, we have expressed t and ν at $z = 0$ instead of the observer frame, which emphasizes that different redshift scalings of the fluxes between the different spectral regimes are a feature of the frame in which frequency and time are expressed. Light curves and spectra can be mapped onto different redshifts in a straightforward manner via a single $(1+z)$ dependency. Finally, also from eq. 2, the dependence on the radiation parameters ϵ_e , ϵ_B and ξ_N remains unchanged at all times.

The fact that observer time t scales the same as t_e and r (that have been integrated over in order to obtain the flux) follows from the $t = t_e - \mu r/c$ constraint that matches different emission times to a single arrival time. In table 1 we have tabulated the effect of applying

F or ν	leading order scalings	κ	λ
$F_{B,BM}$	$(1+z)E_{iso}^{1/2}n_0^{-1/2}\epsilon_e^1\epsilon_B^0\xi_N^{-1}t^{1/2}\nu^2$	$\kappa^{2/3}$	$\lambda^{-2/3}$
$F_{B,ST}$	$(1+z)E_{iso}^{4/5}n_0^{-4/5}\epsilon_e^1\epsilon_B^0\xi_N^{-1}t^{-2/5}\nu^2$		
$F_{D,BM}$	$(1+z)E_{iso}^{5/6}n_0^{1/2}\epsilon_e^{-2/3}\epsilon_B^{1/3}\xi_N^{5/3}t^{1/2}\nu^{1/3}$	κ^1	$\lambda^{1/3}$
$F_{D,ST}$	$(1+z)E_{iso}^{7/15}n_0^{13/15}\epsilon_e^{-2/3}\epsilon_B^{1/3}\xi_N^{5/3}t^{8/5}\nu^{1/3}$		
$F_{E,BM}$	$(1+z)E_{iso}^{7/6}n_0^{5/6}\epsilon_e^0\epsilon_B^1\xi_N^1t^{1/6}\nu^{1/3}$	$\kappa^{11/9}$	$\lambda^{7/9}$
$F_{E,ST}$	$(1+z)E_{iso}^1n_0^1\epsilon_e^0\epsilon_B^1\xi_N^1t^{2/3}\nu^{1/3}$		
$F_{F,BM}$	$(1+z)E_{iso}^{3/4}n_0^0\epsilon_e^0\epsilon_B^{-1/4}\xi_N^1t^{-1/4}\nu^{-1/2}$	$\kappa^{2/3}$	$\lambda^{1/12}$
$F_{F,ST}$	$(1+z)E_{iso}^{1/2}n_0^{1/4}\epsilon_e^0\epsilon_B^{-1/4}\xi_N^1t^{1/2}\nu^{-1/2}$		
$F_{G,BM}$	$(1+z)E_{iso}^{(p+3)/4}n_0^{1/2}\epsilon_e^{p-1}\epsilon_B^{(1+p)/4}\xi_N^{2-p}t^{3(1-p)/4}\nu^{(1-p)/2}$	κ^1	$\lambda^{(1+p)/4}$
$F_{G,ST}$	$(1+z)E_{iso}^{(5p+3)/10}n_0^{(19-5p)/20}\epsilon_e^{p-1}\epsilon_B^{(1+p)/4}\xi_N^{2-p}t^{(21-15p)/10}\nu^{(1-p)/2}$		
$F_{H,BM}$	$(1+z)E_{iso}^{(p+2)/4}n_0^0\epsilon_e^{p-1}\epsilon_B^{(p-2)/4}\xi_N^{2-p}t^{(2-3p)/4}\nu^{-p/2}$	$\kappa^{2/3}$	$\lambda^{(3p-2)/12}$
$F_{H,ST}$	$(1+z)E_{iso}^{(p)/2}n_0^{(2-p)/4}\epsilon_e^{p-1}\epsilon_B^{(p-2)/4}\xi_N^{2-p}t^{(4-3p)/2}\nu^{-p/2}$		
$F_{peak,BM}$	$(1+z)E_{iso}^1n_0^{1/2}\epsilon_e^0\epsilon_B^{1/2}\xi_N^1t^0$	κ^1	$\lambda^{1/2}$
$F_{peak,ST}$	$(1+z)E_{iso}^{4/5}n_0^{7/10}\epsilon_e^0\epsilon_B^{1/2}\xi_N^1t^{3/5}$		
$\nu_{m,BM}$	$E_{iso}^{1/2}n_0^0\epsilon_e^2\epsilon_B^{1/2}\xi_N^{-2}t^{-3/2}$	κ^0	$\lambda^{1/2}$
$\nu_{m,ST}$	$E_{iso}^1n_0^{-1/2}\epsilon_e^2\epsilon_B^{1/2}\xi_N^{-2}t^{-3}$		
$\nu_{c,BM}$	$E_{iso}^{-1/2}n_0^{-1}\epsilon_e^0\epsilon_B^{-3/2}\xi_N^0t^{-1/2}$	$\kappa^{-2/3}$	$\lambda^{-5/6}$
$\nu_{c,ST}$	$E_{iso}^{-3/5}n_0^{-9/10}\epsilon_e^0\epsilon_B^{-3/2}\xi_N^0t^{-1/5}$		
$\nu_{a,BM}$	$E_{iso}^{1/5}n_0^{3/5}\epsilon_e^{-1}\epsilon_B^{1/5}\xi_N^{8/5}t^0$	$\kappa^{1/5}$	$\lambda^{3/5}$
$\nu_{a,ST}$	$E_{iso}^{-1/5}n_0^1\epsilon_e^{-1}\epsilon_B^{1/5}\xi_N^{8/5}t^{6/5}$		

Table 1: Scalings for flux in different spectral regimes, both in the relativistic BM limit and non-relativistic ST limit. Note that t and ν are expressed in the frame where redshift $z = 0$. In the observer frame, $\nu_{\oplus} = \nu/(1+z)$ and $t_{\oplus} = t(1+z)$. The κ and λ columns denote the corresponding scaling of the flux under a scaling of energy, time and density according to eq. 3. The scaling of ν_a applies to the case where $\nu_a < \nu_m < \nu_c$.

the mapping

$$\begin{aligned} E'_{iso} &= \kappa E_{iso}, \\ n'_0 &= \lambda n_0, \\ t' &= (\kappa/\lambda)^{1/3} t, \end{aligned} \tag{3}$$

to the observed flux. This scaling remains unchanged between early time BM and late time ST for all spectral regimes, e.g. $F'_{D,BM}/F_{D,BM} = F'_{D,ST}/F_{D,ST} = \kappa\lambda^{1/3}$, independent of jet opening angle or observer angle.

3. Numerical verification

Fig. 2 demonstrates that the scaling between energies applies at all times. The light curves remain in spectral regime G throughout their evolution, so $F'(E'_{iso}, t') = \kappa F(E_{iso}, t)$. All light curves were taken from the dataset used in Van Eerten & MacFadyen (2011), available from the on-line afterglow library at <http://cosmo.nyu.edu/afterglowlibrary>.

To generate light curves that do not lie on the asymptote of a single spectral regime we need to take the spectral evolution into account. As shown in table 1, both the critical frequencies and peak fluxes obey the same scalings throughout the blast wave evolution. Therefore, once we know their time evolution for a given set of parameters (E_{iso} , n_0 , θ_0) we can use these as a baseline to generate the connected power-law spectra for arbitrary values of the jet parameters. In Fig. 3 we plot the time evolution of F_{peak} , ν_c , ν_m for $\theta_0 = 0.2$ rad and an on-axis observer. They have been calculated using the methods presented in Van Eerten et al. (2011) and are ultimately based on the simulations described therein. All simulations were performed using the RAM adaptive-mesh refinement (AMR) relativistic hydrodynamics (RHD) code (Zhang & MacFadyen 2006). For details, see Van Eerten et al. (2011).

At early times ν_c and F_{peak} differ numerically from their asymptotically expected time evolution because the blast wave is initially underresolved in the RHD simulations. However, all explosion energy is included in the initial conditions of the simulations, and the resulting drop in blast wave Lorentz factor is temporary (for more details, see Van Eerten et al. 2011; Zhang & MacFadyen 2009). But initially the observed flux level and critical frequencies are impacted due to the temporary decrease in beaming. However, the scalability of the jet dynamics justifies the computational cost of extremely high resolution blast wave simulations and these will be presented in future work.

For jet half-opening angle $\theta_0 = 0.2$, a jet break occurs around ~ 10 days. As a result,

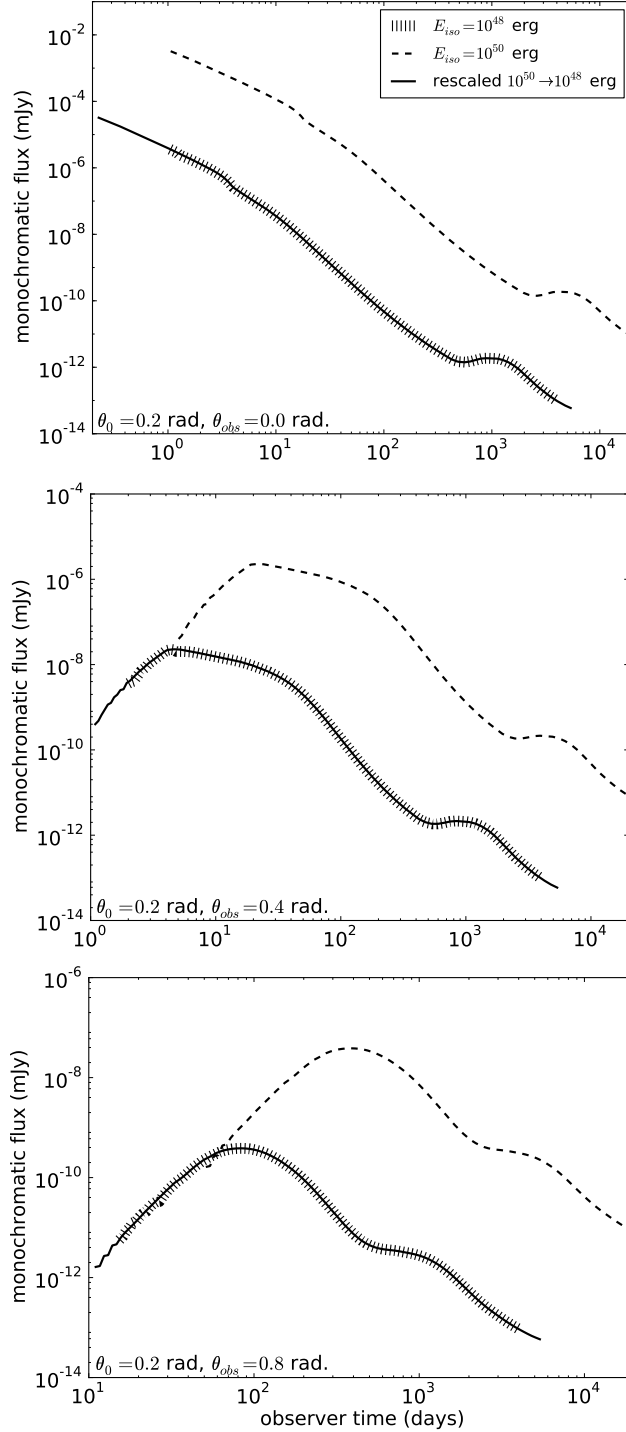


Fig. 2.— Demonstrations of scaling between optical light curves ($\nu = 4.56 \times 10^{14}$ Hz) with $E_{iso} = 10^{48}$ erg and $E_{iso} = 10^{50}$ erg, for different observer angles θ_{obs} . Other parameters are set as follows: $n_0 = 10^{-3} \text{ cm}^{-3}$, $\theta_0 = 0.2$ rad, $p = 2.5$, $\epsilon_B = 0.01$, $\epsilon_e = 0.1$, $\xi_N = 1.0$, $z = 0$, $d_L = 10^{28}$ cm. The legend in the top plot refers to all plots.

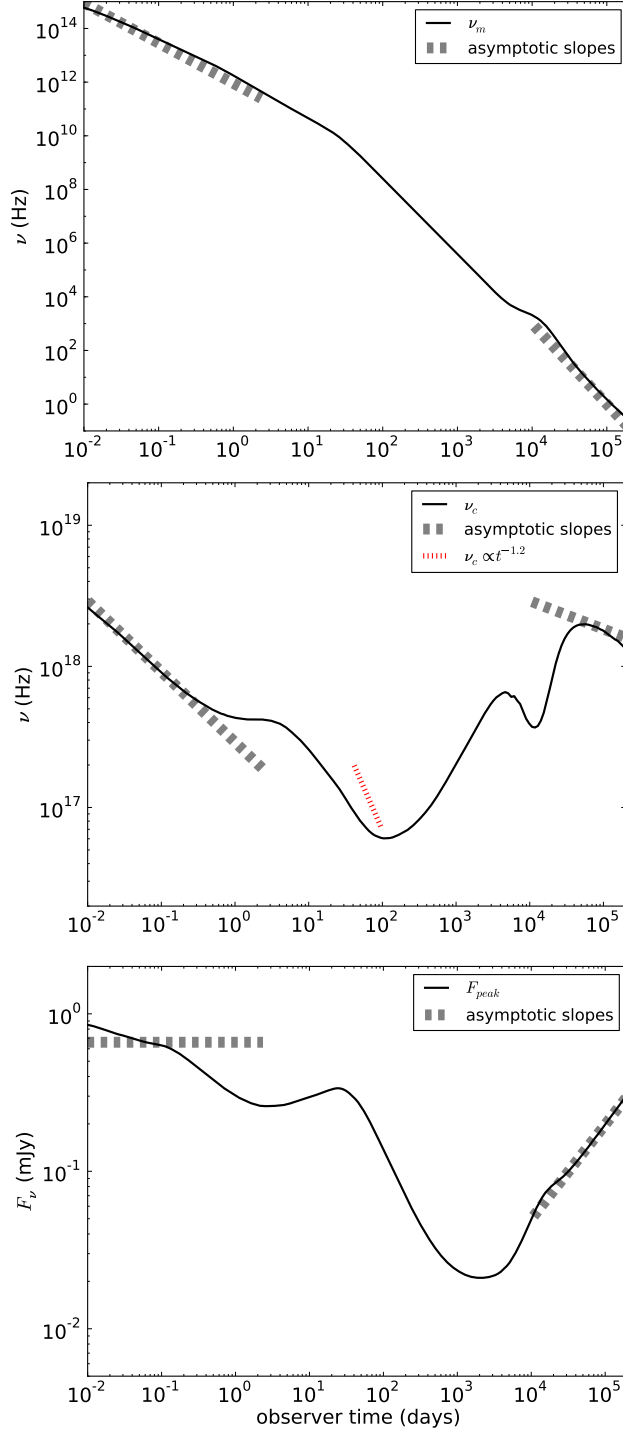


Fig. 3.— Evolution of critical quantities for on-axis observers. The following parameters were used: $E_{iso} = 5 \times 10^{52}$ erg, $n_0 = 10^{-3}$ cm $^{-3}$, $\theta_0 = 0.2$ rad, $p = 2.5$, $\epsilon_B = 0.01$, $\epsilon_e = 0.1$, $\xi_N = 1.0$, $z = 0$, $d_L = 10^{28}$ cm. From top to bottom, the plots show ν_m , ν_c and F_{peak} . The BM and ST asymptotic slopes are indicated by dashed lines. The dotted line in the center of the ν_c plot indicates the temporal slope of ν_c found by Filgas et al. (2011) for GRB 091127.

the time evolutions change significantly. The temporal slope of ν_m turns over quickly from $\nu_m \propto t^{-3/2}$ (BM) to the far steeper ST slope $\nu_m \propto t^{-3}$. The temporal slope for ν_c is not only less steep at late times, its late time ST asymptote also lies significantly higher than the early time BM asymptote, and as a result ν_c actually *rises* for some time after the jet break. This effect will be less severe for larger opening angles, since $\nu_c \propto E_{iso}^{-3/5}$ in the BM regime and $\nu_c \propto E_j^{-3/5}$ in the ST regime, where E_j the total energy in both jets (and therefore in the final ST sphere). The two energies are related via $E_j \approx E_{iso}\theta_0^2/2$. It is also worth noting that, before rising, the temporal slope of ν_c temporarily *steepens* beyond $-1/2$. A steepening of the cooling break frequency to $\nu_c \propto t^{-1.2}$ has recently been observed in GRB 091127 by comparing optical and X-ray data (Filgas et al. 2011). Our plot shows that this is, in principle, not inconsistent with simulations (and therefore with the standard model, since we do not expand upon the standard synchrotron framework by including features like evolving microphysics parameters such as ϵ_B). However, we caution against overinterpretation of the post-break ν_c evolution because our approach to electron cooling (based on Sari et al. 1998) relies on a single global cooling time approximation rather than on tracing the local accelerated electron distribution (for a comparison between the two approaches, see Van Eerten et al. 2010. In the example there, ν_c for local cooling is typically higher by a factor ~ 5). Given this caveat for ν_c , a clear steepening of ν_m and ν_c immediately post jet break is a general prediction of our study, with the steepening of ν_m being more robust.

The final feature in all three evolution plots is the onset of the counterjet around ~ 250 days, resulting in a relative increase of F_{peak} and ν_m and a decrease in ν_c . This effect is strongest around ~ 1500 days.

Using both the on-axis baselines shown in Fig 3 and the baselines for $\theta_0 = 0.2$ rad, $\theta_{obs} = 2\theta_0/3$, we have generated spectra (excluding synchrotron self-absorption) for a different set of explosion and radiation parameters and compare these to spectra calculated directly from simulations. The results are shown in Fig 4. The off-axis angle is equal to the average observer angle assuming randomly oriented jets and no detection if $\theta_{obs} > \theta_0$. The scaling approach correctly captures the peak flux and break frequencies. The scalings-based spectra can be further improved upon by including smooth power law transitions between different spectral regimes. Fig 3 suggests that some dependency on θ_{obs} is to be expected.

4. Summary and Discussion

We show that gamma-ray burst afterglow spectra and light curves above the synchrotron self-absorption break can be generated for arbitrary explosion and radiation parameters by

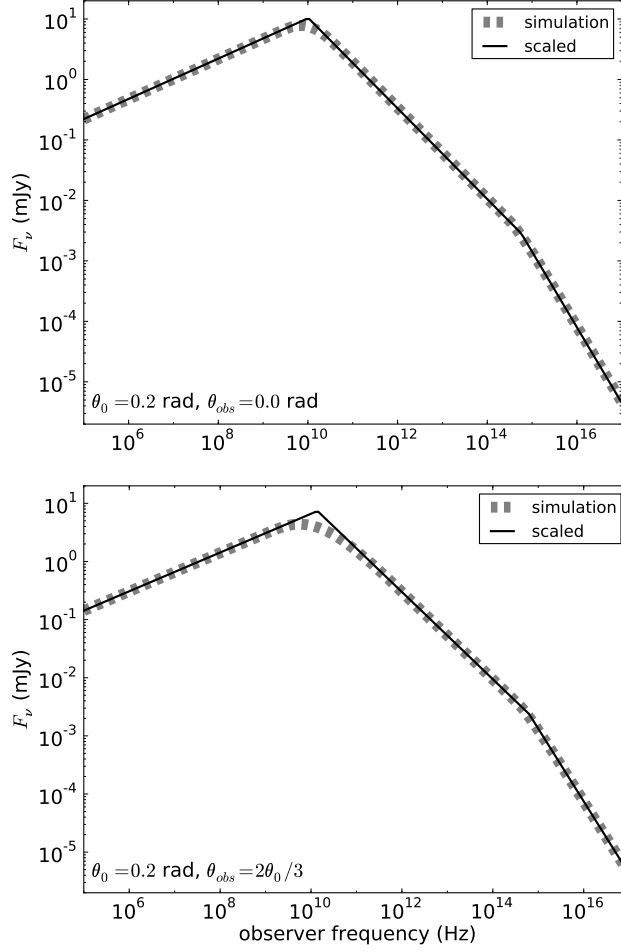


Fig. 4.— Comparison between simulation and scalings based spectra. The following parameters are used for the spectra: $E_{iso} = 35 \times 10^{52} \text{ erg}$, $n_0 = 11 \times 10^{-3} \text{ cm}^{-3}$, $\theta_0 = 0.2 \text{ rad}$, $p = 2.5$, $\epsilon_B = 0.03$, $\epsilon_e = 0.1$, $\xi_N = 1.0$, $z = 0$, $d_L = 10^{28} \text{ cm}$. The top plot shows a spectrum viewed on-axis, the bottom plot shows the spectrum observed from the average expected observer angle. The spectra are taken at an observer time $t = 43 \text{ days}$.

scaling the values of a few key parameters (F_{peak} , ν_c , ν_m) from a given baseline. The baseline only needs to be calculated once for each observer and jet collimation angle. In the current study we have used sharp transitions between the different spectral regimes, but smooth power law transitions can be parametrized (e.g. following Granot & Sari 2002). Although we have confined our study to a homogeneous circumburst environment, the generalization to a stellar wind environment is straightforward and will be presented in future work. The blast waves initially follow the ultra-relativistic Blandford-McKee self-similar solution and gradually spread out to the late time non-relativistic Sedov-von Neumann-Taylor stage.

We plot the time evolution of the key parameters F_{peak} , ν_m , ν_c and the plots reveal that the critical frequencies are strongly affected by the jet break. After the jet break, the ν_m temporal slope quickly drops to the steep late time Sedov-Taylor slope $\nu_m \propto t^{-3}$, while the cooling break ν_c first steepens then rises to meet the level of its late time asymptote. The steepening of the temporal slope of ν_c has been observed for GRB 091127 (Filgas et al. 2011), though we caution against overinterpretation of our results given our simplified approach to electron cooling using a global cooling time (following Sari et al. 1998).

The scaling-based light curves fully include all two-dimensional dynamical features of expanding and decelerating afterglow blast waves. The fact that light curves can now be instantly generated for the standard synchrotron afterglow model, while taking realistic dynamics into account, has the potential to strongly impact afterglow light curve fitting. In future work, we will implement the time evolution of key parameters for a wide range of observer and jet collimation angles into a fit code that will be made available for download on <http://cosmo.nyu.edu/afterglowlibrary>. Our findings imply that it is now possible in principle to fully fit for the shape of the jet break (e.g. at early time X-ray and optical frequencies, see Evans et al. 2009; Racusin et al. 2009 for examples from *Swift*). More generally, the accuracy of different parametrizations of the jet break transition (Beuermann et al. 1999; Harrison et al. 1999) can be assessed. With the general shape of the transition into the ST regime being known for arbitrary explosion parameters, the exact moment when the ST asymptote is reached in the light curve (see e.g. Livio & Waxman 2000; Wygoda et al. 2011) is no longer relevant, which will improve late time radio calorimetry (see e.g. Berger et al. 2004; Shivvers & Berger 2011).

In this work we have not discussed synchrotron self-absorption in detail, but we do show that the critical frequency ν_a obeys the same scaling relations as the other key parameters. The effect of self-absorption will be investigated in a follow-up study. Although the scaling of ν_a is encouraging from the perspective of broadband afterglow fitting, features such as the chromaticity of the jet-break across the self-absorption break (van Eerten et al. 2011) might impact the spectral slope and the sharpness of the transition into the self-absorption

spectral regime, rendering a parametrization slightly more complex.

In our previous study (Van Eerten et al. 2011) we presented a method to quickly calculate light curves based on scalings on the level of the jet dynamics. This method had the disadvantage that a full radiative transfer was still required for each datapoint. As a result, broadband afterglow fitting-based on this approach still requires use of a large parallel computer in practice. The current method no longer requires radiative transfer calculations and is therefore vastly superior in terms of computational cost. Nevertheless, in two key aspects the ‘BOX-based’ framework from Van Eerten et al. (2011) remains relevant. First, since the scalings there happen on the level of the dynamics, no parametrizations are necessary in order to describe the transitions between different spectral regimes and smoothly connected power laws emerge naturally. Second, the scalable BOX-based blast wave dynamics data provide a testing lab for studying the effect of various radiative processes, while the current study takes synchrotron radiation as its starting point.

This research was supported in part by NASA through grant NNX10AF62G issued through the Astrophysics Theory Program and by the NSF through grant AST-1009863. The software used in this work was in part developed by the DOE-supported ASCI/Alliance Center for Astrophysical Thermonuclear Flashes at the University of Chicago. We thank Alexander van der Horst and Andrei Gruzinov for helpful comments.

REFERENCES

- Berger, E., Kulkarni, S. R., & Frail, D. A. 2004, *ApJ*, 612, 966
- Beuermann, K., Hessman, F. V., Reinsch, K., Nicklas, H., Vreeswijk, P. M., Galama, T. J., Rol, E., van Paradijs, J., Kouveliotou, C., Frontera, F., Masetti, N., Palazzi, E., & Pian, E. 1999, *A&A*, 352, L26
- Blandford, R. D., & McKee, C. F. 1976, *Physics of Fluids*, 19, 1130
- Downes, T. P., Duffy, P., & Komissarov, S. S. 2002, *MNRAS*, 332, 144
- Eichler, D., Livio, M., Piran, T., & Schramm, D. N. 1989, *Nature*, 340, 126
- Evans, P. A., Beardmore, A. P., Page, K. L., Osborne, J. P., O’Brien, P. T., Willingale, R., Starling, R. L. C., Burrows, D. N., Godet, O., Vetere, L., Racusin, J., Goad, M. R., Wiersema, K., Angelini, L., Capalbi, M., Chincarini, G., Gehrels, N., Kennea, J. A.,

- Margutti, R., Morris, D. C., Mountford, C. J., Pagani, C., Perri, M., Romano, P., & Tanvir, N. 2009, MNRAS, 397, 1177
- Filgas, R., Greiner, J., Schady, P., Krühler, T., Updike, A. C., Klose, S., Nardini, M., Kann, D. A., Rossi, A., Sudilovsky, V., Afonso, P. M. J., Clemens, C., Elliott, J., Nicuesa Guelbenzu, A., Olivares E., F., & Rau, A. 2011, A&A, 535, A57
- Frail, D. A., Waxman, E., & Kulkarni, S. R. 2000, ApJ, 537, 191
- Granot, J., & Sari, R. 2002, ApJ, 568, 820
- Granot, J., & Piran, T. 2011, ArXiv e-prints: 1109.6468
- Harrison, F. A., Bloom, J. S., Frail, D. A., Sari, R., Kulkarni, S. R., Djorgovski, S. G., Axelrod, T., Mould, J., Schmidt, B. P., Wieringa, M. H., Wark, R. M., Subrahmanyam, R., McConnell, D., McCarthy, P. J., Schaefer, B. E., McMahon, R. G., Markze, R. O., Firth, E., Soffitta, P., & Amati, L. 1999, ApJ, 523, L121
- Huang, Y. F., Dai, Z. G., & Lu, T. 1999, MNRAS, 309, 513
- Livio, M., & Waxman, E. 2000, ApJ, 538, 187
- MacFadyen, A. I., & Woosley, S. E. 1999, ApJ, 524, 262
- Meszáros, P., & Rees, M. J. 1997, ApJ, 476, 232
- Paczynski, B. 1991, Acta Astron., 41, 257
- Panaitescu, A., & Kumar, P. 2002, ApJ, 571, 779
- Racusin, J. L., Liang, E. W., Burrows, D. N., Falcone, A., Sakamoto, T., Zhang, B. B., Zhang, B., Evans, P., & Osborne, J. 2009, ApJ, 698, 43
- Rhoads, J. E. 1999, ApJ, 525, 737
- Sari, R., Piran, T., & Narayan, R. 1998, ApJ, 497, L17+
- Sedov, L. I. 1959, Similarity and Dimensional Methods in Mechanics (Similarity and Dimensional Methods in Mechanics, New York: Academic Press, 1959)
- Shivvers, I., & Berger, E. 2011, ApJ, 734, 58
- Taylor, G. 1950, Royal Society of London Proceedings Series A, 201, 159

- van Eerten, H. J., Leventis, K., Meliani, Z., Wijers, R. A. M. J., & Keppens, R. 2010, MNRAS, 403, 300
- van Eerten, H., Zhang, W., & MacFadyen, A. 2010, ApJ, 722, 235
- van Eerten, H. J., Meliani, Z., Wijers, R. A. M. J., & Keppens, R. 2011, MNRAS, 410, 2016
- van Eerten, H. J., & MacFadyen, A. I. 2011, ApJ, 733, L37
- van Eerten, H. J., & MacFadyen, A. I. 2011, ArXiv e-prints: 1105.2485
- van Eerten, H. J., van der Horst, A. J., & MacFadyen, A. I. 2011, ApJ Submitted. ArXiv e-prints: 1110.5089
- Von Neumann, J. 1961, Collected works, ed. von Neumann, J.
- Wijers, R. A. M. J., Rees, M. J., & Meszaros, P. 1997, MNRAS, 288, L51
- Wijers, R. A. M. J., & Galama, T. J. 1999, ApJ, 523, 177
- Woosley, S. E. 1993, ApJ, 405, 273
- Wygoda, N., Waxman, E., & Frail, D. A. 2011, ApJ, 738, L23
- Zhang, W., & MacFadyen, A. I. 2006, ApJS, 164, 255
- Zhang, W., & MacFadyen, A. 2009, ApJ, 698, 1261